Since January 2020 Elsevier has created a COVID-19 resource centre with free information in English and Mandarin on the novel coronavirus COVID-19. The COVID-19 resource centre is hosted on Elsevier Connect, the company's public news and information website.

diabetesresearchandclinicalpractice197(2023)110565

Contents lists available at ScienceDirect

Diabetes Research and Clinical Practice

journal homepage: www.journals.elsevier.com/diabetes-research-and-clinical-practice

Extracellular vesicle proteomics and phosphoproteomics identify pathways for increased risk in patients hospitalized with COVID-19 and type 2 diabetes mellitus

Yury O. Nunez Lopez [a,1], Anton Iliuk [b,c,*,1], Anna Casu [a], Amay Parikh [d], Joshua S. Smith [a], Karen Corbin [a], Daniel Lupu [a], Richard E. Pratley [a,*]

[a] Translational Research Institute, AdventHealth Orlando, Orlando, FL 32804, United States
[b] Department of Biochemistry, Purdue University, West Lafayette, IN 47907, United States
[c] Tymora Analytical Operations, West Lafayette, IN 47906, United States
[d] Division of Critical Care, AdventHealth Medical Group, AdventHealth Orlando, Orlando, FL 32804, United States

ARTICLE INFO

Keywords:
COVID-19
Type 2 diabetes mellitus
Acute respiratory disease
Hospitalized patient
COVID-19 and diabetes interaction
Extracellular vesicle
Exosome
Proteomics
Phosphoproteomics

ABSTRACT

Recent studies suggest that extracellular vesicles (EVs) play a role in the pathogenesis of SARS-CoV-2 infection and the severity of COVID-19. However, their role in the interaction between COVID-19 and type 2 diabetes (T2D) has not been addressed. Here, we characterized the circulating EV proteomic and phosphoproteomic landscape in patients with and without T2D hospitalized with COVID-19 or non-COVID-19 acute respiratory illness (RSP). We detected differentially expressed protein and phosphoprotein signatures that effectively characterized the study groups. The trio of immunomodulatory and coagulation proteins C1QA, C1QB, and C1QC appeared to be a central cluster in both the COVID-19 and T2D functional networks. PKCβ appeared to be retained in cells by being diverted from EV pathways and contribute to the COVID-19 and T2D interaction via a PKC/BTK/TEC axis. EV-shuttled CASP3 and ROCK1 appeared to be coregulated and likely contribute to disease interactions in patients with COVID-19 and T2D. Predicted activation of AMPK, MAPK, and SYK appeared to also play important roles driving disease interaction. These results suggest that activated cellular kinases (i.e., PKC, AMPK, MAPK, and SYK) and multiple EV-shuttled kinases (i.e., PKCβ, BTK, TEC, MAP2K2, and ROCK1) may play key roles in severe COVID-19, particularly in patients with comorbid diabetes.

1. Introduction

Adults with type 2 diabetes mellitus (T2D) are at increased risk for severe COVID-19, but the specific mechanisms heightening risk remain to be fully elucidated [1,2]. It is suggested that a reciprocal and detrimental interaction between the immune and endocrine system drives this interaction [1,2]. Extracellular vesicles (EVs) are key players in intercellular and interorgan communication in both normal physiology and disease pathogenesis. In COVID-19, several studies suggest that EVs play a role in the pathogenesis of SARS-CoV-2 infection and severity of COVID-19 [3–8]. Platelet-derived EVs, for example, were found to be elevated in multiple cohorts [4,5]. EV proteins involved in inflammation, coagulation, and immunomodulation were suggested to contribute to SARS-CoV-2 infection [6]. In hospitalized COVID-19 patients, alterations in these proteins may contribute to severe disease [7]. More recently, using state-of-the-art imaging flow cytometry, Tertel and colleague found that $CD24^+$ EV subpopulations were enriched in people with mild symptoms, while CD82 + EVs were enriched in people with severe symptoms [8]. CD24 is a marker of several B cell subtypes including regulatory B cells and the presence of these cells has been associated with the duration of COVID-19 symptoms [9,10]. On the other hand, $CD82^+$ EVs correlated with the frequency of circulating IL-6-producing myeloid-derived suppressor cells [8]. Importantly, the quantification of $CD82^+$ and $CD24^+$ EVs displayed better performance by linear discriminant effect size (LEfSe) analysis as indicators for severe COVID-19, as compared to previously known biomarkers such as the number of circulating neutrophils and myeloid-derived suppressor cells (MDSCs) or the concentration of various pro-inflammatory markers (e.

* Corresponding authors.
E-mail addresses: anton.iliuk@tymora-analytical.com (A. Iliuk), Richard.Pratley.MD@AdventHealth.com (R.E. Pratley).
[1] These authors contributed equally.

https://doi.org/10.1016/j.diabres.2023.110565
Received 18 October 2022; Received in revised form 22 January 2023; Accepted 30 January 2023
Available online 1 February 2023

g., C-reactive protein, D-dimer, interleukin IL-8) in the blood [8].

Beyond COVID-19, EVs have been more extensively studied in T2D. Several studies suggest that both the proteome and the mirnome (miRNAs) of EVs from patients with diabetes have proinflammatory proprieties, which we reason, could indirectly contribute to the severity of COVID-19 when both diseases co-occur [11–19]. Prattichizzo and colleagues, for example, recently provided evidence that a specific subpopulation of EVs characterized by the expression of the surface marker platelet endothelial cell adhesion molecule 1 (PECAM1/CD31), derived from platelets, immune cells, and endothelial cells, can promote proinflammatory pathways in targeted endothelial cells [16,17]. These $CD31^{+}$ EVs shuttled a specific diabetic microRNA signature that was able to effectively discriminate T2D patients with complications from T2D patients without complications including diabetic retinopathy, nephropathy, neuropathy, ischemic heart disease, and peripheral vascular disease [16,17]. In a study of the proteomic and phosphoproteomic landscape of circulating EVs in subjects with prediabetes, T2D and normal glucose tolerance we identified a potential role of protein kinase C as a driver of upstream phosphorylation events that define phosphoproteomic signatures in prediabetes and T2D.[19] We reasoned that circulating EVs from patients with dysglycemia distribute activated kinases that alter relevant signaling pathways in target tissues and ultimately contribute to diabetes development and progression.

To gain insight into EV-mediated molecular mechanisms potentially driving the COVID-19 and T2D interaction and to identify potential biomarkers or therapeutic targets in this context, we compared the proteomic and phosphoproteomic profiles of circulating EVs in 48 hospitalized patients selected to create 4 matched groups of those with and without T2D and with either COVID-19 or non-COVID-19 acute respiratory illness (RSP).

2. Materials and methods

2.1. Study approval

All aspects of the study were approved by the Institutional Review Board of AdventHealth. Deidentified plasma samples were obtained from the clinical laboratory and matched to clinical data through an honest broker system.

2.2. Study cohorts

Study participants were identified from a set of 494 patients hospitalized at AdventHealth Orlando with a COVID-19 (SARS-CoV-2 PCR positive) or alternative (SARS-CoV-2 PCR negative) acute respiratory infection (RSP) diagnosis during June-August 2020 and for which plasma samples were available in our biorepository. Patients with type 1 diabetes, pregnant women, or those admitted directly into the ICU were excluded. To generate four balanced groups, 10,000 random cohorts were automatically generated and differences among variables assessed using the Fisher test for categorical variables and ANOVA for continuous variables. Random cohorts were constrained by an equal number of males and females from each race ethnicity per group, whenever possible. When the number of Hispanic/Latino (H/L) or African American (AA) female or male participants per group was limited, non-Hispanic white (NHW) females or males were used as substitutes, respectively. Random cohorts were ranked by the averaged P value for several key comparisons including age, lag-time (time samples remained stored at 4 °C before long-term storage at −80 °C in the biorepository), and time difference between sample collection and hospitalization (constrained to a maximum of 5 days).

2.3. EV isolation

EV purification was conducted as described by Nunez Lopez and colleagues [19], using EVtrap™ (Tymora Analytical, Lafayette, IN, USA), a non-antibody- bead-based affinity technology developed to specifically and quantitatively isolate EVs. The EVtrap™ technology has been further described and validated in detail elsewhere [19–28]. In short, frozen plasma samples were thawed and large debris removed by centrifugation at 2500 × g for 10 min. The pre-cleared plasma was then diluted 20-fold in PBS and incubated with EVtrap™ beads for 30 min. The magnetic beads were captured using a magnetic separator rack, then washed with PBS, and the EVs eluted with 200 mM triethylamine (TEA, Millipore-Sigma). The resulting EV samples were fully dried in vacuum centrifuge.

2.4. Mass spectrometry (LC-MS/MS)-based methods used to detect the global EV proteome and phosphoproteome

LC-MS was conducted as described by Nunez Lopez and colleagues [19]. Briefly, EVs were solubilized in lysis solution then diluted fivefold with 50 mM triethylammonium bicarbonate and digested with Lys-C (Wako) at 1:100 (wt/wt) enzyme-to-protein ratio for 3 h at 37 °C. Trypsin was added to a final 1:50 (wt/wt) enzyme-to-protein ratio for overnight digestion at 37 °C. After surfactant removal, the resulting peptides were desalted using Top-Tip C18 tips (Glygen, Columbia, MD, USA) according to manufacturer's instructions. The samples were dried completely in a vacuum centrifuge and dissolved at 0.1 μg/μL in 0.05% trifluoroacetic acid with 3% (vol/vol) acetonitrile. For phosphoproteome analysis, the 99% portion of each sample was subjected to phosphopeptide enrichment using PolyMAC Phosphopeptide Enrichment kit (Tymora Analytical,West Lafayette, IN, USA) according to the manufacturer's instructions, and the eluted phosphopeptides dried completely in a vacuum centrifuge. For phosphoproteomics analysis, the whole enriched sample was used, while for proteomics, only 50% of the sample was loaded onto the LC-MS. Each dried peptide or phosphopeptide sample was dissolved at 0.1 μg/μL in 0.05% trifluoroacetic acid with 3% (vol/vol) acetonitrile. A total of 10 μL of each sample was injected into an Ultimate 3000 nano UHPLC system (Thermo Fisher Scientific, Waltham, MA, USA) and peptides captured on a 2 cm Acclaim PepMap trap column and separated on a heated 50 cm column packed with ReproSil Saphir 1.9 μm C18 beads (Dr. Maisch GmbH, Ammerbuch, Germany). The mobile phase buffer consisted of 0.1% formic acid in ultrapure water (buffer A) with an eluting buffer of 0.1% formic acid in 80% (vol/vol) acetonitrile (buffer B) run with a linear 60 min gradient of 6–30% buffer B at a flow rate of 300 nL/min. The UHPLC was coupled online with a Q-Exactive HF-X mass spectrometer (Thermo Fisher Scientific, Waltham, MA, USA). The mass spectrometer was operated in the data-dependent mode, in which a full-scan MS (from m/z 375 to 1500 with a resolution of 60,000) was followed by MS/MS of the 15 most intense ions (30,000 resolution; normalized collision energy—28%; automatic gain control target (AGC)—2E4, maximum injection time—200 ms; 60 sec exclusion).

2.5. Bioinformatic analysis of MS/MS data

Raw MS/MS data was analyzed as described by Nunez Lopez and colleagues [19]. In short, peptides were searched directly against the human Uniprot database with no redundant entries, using Byonic (Protein Metrics, Cupertino, CA, USA) and Sequest search engines loaded into Proteome Discoverer 2.3 software (Thermo Fisher Scientific, Waltham, MA, USA). MS1 precursor mass tolerance was set at 10 ppm, and MS2 tolerance was set at 20 ppm. Search criteria included a static carbamidomethylation of cysteines (+57.0214 Da), variable modifications of oxidation (+15.9949 Da) on methionine residues, acetylation (+42.011 Da) at the N terminus of proteins, and phosphorylation of S, T, and Y residues (+79.996 Da) for the phosphoproteomics data. The search was performed with full trypsin/P digestion and allowed a maximum of two missed cleavages on the peptides analyzed from the sequence database. The false discovery rates of proteins and peptides were set at 0.01. All protein and peptide identifications were grouped,

and any redundant entries were removed. Only unique peptides and unique master proteins were reported. All data were quantified using the label-free quantitation node of Precursor Ions Quantifier through the Proteome Discoverer v2.3 (Thermo Fisher Scientific, Waltham, MA, USA). For the quantification of proteomic or phosphoproteomic data, the intensities of peptides/phosphopeptides were extracted with initial precursor mass tolerance set at 10 ppm, minimum number of isotope peaks as 2, maximum ΔRT of isotope pattern multiplets—0.2 min, PSM confidence FDR of 0.01, with hypothesis test of ANOVA, maximum RT shift of 5 min, pairwise ratio-based ratio calculation, and 100 as the maximum allowed fold change. The abundance levels of all peptides and proteins were normalized using the total peptide amount normalization node in the Proteome Discoverer.

2.6. Phosphosite-centric analyses

Phosphosite level analysis was conducted using the R package *PhosR* [29, 30] as described by Nunez Lopez and colleagues [19]. In brief, the code for processing and downstream analyses of phosphoproteomic data was adapted from reference [29]. Up-stream kinases responsible for detected phosphorylation signatures are identified and potential novel kinase-substrate pairs and global relationships between kinases are predicted. Phosphosite filtering (forced to be present in at least 50% of the samples from one study group) and imputation (site and condition-specific imputation with scImpute using 50% as quantification rate threshold per condition and tail-base imputation with tImpute functions) was performed. Quantile normalization of the imputed data and differential phosphosite expression analysis was done using linear models and moderated empirical Bayes statistics implemented in the *limma* R package [31]. Kinase perturbation analysis was conducted using the perturbPlot2d function from the *directPA* R package [32]. The PhosphoSitePlus annotation database was used as the source of kinase-substrate annotations.

2.7. Nanoparticle tracking analysis (NTA)

The size distribution and concentration of particles in EV preparations were analyzed using dynamic light-scattering technology with a NanoSight NS300 instrument and NTA-3.4 software (Malvern Panalytical, Malvern). The instrument was equipped with a 488 nm blue laser module, flow-cell top plate, integrated temperature control, and a single-syringe pump module. Samples were diluted using cell culture grade water (Corning cat# 25-005-CI) to produce an optimal particle concentration for final measurement in the range of 10^7 to 10^9 particles/ml. Dilutions were initially assessed with a single quick static measurement of 30 s to identify the optimal dilution (which represented approximately 20 to 100 particles in the instrument's field of view, per video frame). For final, more accurate quantification, 5 standard measurements of 1 min of duration each were taken at a controlled temperature of 25 °C and under constant automatic flow (continuous syringe pump speed set to 50 arbitrary units). Camera level for video capture was set to 12 and detection threshold to 5 for all sample measurements.

2.8. Statistical analysis

Data normality was tested using the Shapiro-Wilk test, and non-normal data was log-transformed to approximate normality. Differences in baseline clinical characteristics were assessed using the Welch two-sample *t* test (for continuous variables) or the Fisher exact test (for categorical variables). The multidimensional scaling (MDS) plot were generated with the plotMDS function of the *limma* R package. MDS displays the Euclidean distances among cohorts based on the normalized abundance levels of all stringently detected EV proteins. Differential expression analysis was conducted using the *limma* R package [31]. Data was adjusted for the potential confounding effects of age, gender, race, and ethnicity. Partial correlations were also calculated in the R environment adjusting for the same confounders. Calculated effects and correlations with two-tailed P values < 0.05 were considered significant. False discovery rates (FDR) correcting for multiple testing were calculated using the Benjamini-Hochberg (BH) correction as implemented for the p.adjust function in the *stats* R package. Enrichment for KEGG pathway signatures among the lists of differentially expressed EV proteins was assessed using *clusterProfiler* [33] with a $p < 0.05$ and adjusted $p < 0.1$ as thresholds for statistical significance.

3. Results

3.1. Participants and study design

As described in the materials and methods section, important efforts were made to ensure the homogeneity of the study cohort. The clinical characteristics of the study cohort are summarized in Table 1. The study design allowed us to effectively model and quantify the independent effects of COVID-19 and T2D as well as the interaction between the two diseases. This is, to our knowledge, the first EV proteomic and phosphoproteomic study that controls COVID-19 effects against non-COVID-19 acute respiratory illness (RSP).

3.2. EV preparations are enriched in exosomal particles

To characterize the protein composition of plasma EV preparations purified using Tymora's non-antibody-based affinity EVtrap™ proprietary technology (designed to quantitatively capture membrane-bound vesicles including exosomes and validated in multiple peer-reviewed publications [19–28]), we assessed the enrichment in exosomal proteins curated by the ExoCarta Database. EVs were highly enriched in exosomal proteins, including 87 of the top 100 Exocarta proteins and nanoparticle tracking analysis (NTA) demonstrated size distributions consistent with preparations enriched in small EVs (Fig. 1A-E). Increased particle concentration was evident across most of the size range for the COVID-19 groups compared to their respective non-COVID-19 controls. However, the increase was not statistically significant (Fig. 1E). We further characterized our EV preparations using state-of-the-art LC-MS/MS mass spectrometry. Fig. 1F presents a digital Western-like rendering of proteomic data for classical exosomal markers (namely ALIX, HSP70, FLOT1, Annexin-V, CD63, and CD9, RAB7; boxplots presented in Supplementary Figure SF1), some of which (i.e., Annexin-V/ANXA5 and RAB7) demonstrated significant ($FC > 2$, $P < 0.05$, $FDR < 0.05$) dysregulation in EVs from the COVID-19 groups, as compared to the non-COVID-19 RSP controls (Supplementary Tables ST1-ST2, Supplementary Figure SF1A,F). Interestingly, negative control marker Calnexin/CANX was also significantly affected by COVID-19 (Supplementary Table ST1, Supplementary Figure SF1G).

3.3. EV proteomic and phosphoproteomic signatures effectively distinguished all study groups

To identify potential EV biomarkers contributing to the increased risk of hospitalization in patients with COVID-19 and T2D, we conducted differential expression analysis of the global proteomic and phosphoproteomic data. The differential expression analysis included a COVID-19-by-T2D interaction term in the multivariate models that allowed dissection of the independent effects of each disease on the EV proteome and identified changes that depended on the co-occurrence of both diseases (Supplementary Tables ST1-ST6). For phosphoproteomics analysis, the sample volume available was limited and we were required to make pools of 3 plasma samples each, for a total of 4 pools per study group that represented 16 sample pools in total. Because of this reduction in effective sample size and because the groups were well balanced by design, we did not adjust the models used to analyze the phosphoproteomic data. Results from the differential phosphoproteomic

Table 1
Clinical characteristics of the study cohort.

	Group 1 COV^+T2D^+	Group 2 COV^+T2D^-	Group 3 RSP^+T2D^+	Group 4 RSP^+T2D^-	p
n	12	12	12	12	
COVID Diagnosis = Positive(%)	12 (100.0)	12 (100.0)	0 (0.0)	0 (0.0)	<0.001
T2D Diagnosis = Positive (%)	12 (100.0)	0 (0.0)	12 (100.0)	0 (0.0)	<0.001
RSP Diagnosis = Positive (%)	0 (NaN)	0 (NaN)	12 (100.0)	12 (100.0)	NA
Age / year	69.75 (13.45)	67.17 (18.02)	71.50 (13.74)	68.00 (13.22)	0.892
BMI / kg/m^2	26.60 (7.56)	27.81 (5.52)	31.05 (13.87)	29.75 (9.01)	0.674
Height / cm	169.76 (14.64)	171.24 (12.61)	174.34 (12.30)	168.91 (9.60)	0.74
Actual Weight / kg	77.35 (27.45)	83.10 (26.63)	92.52 (51.61)	84.57 (24.68)	0.756
Patient Gender = Male (%)	6 (50.0)	6 (50.0)	6 (50.0)	6 (50.0)	1
Patient Race = White (%)	6 (50.0)	8 (66.7)	8 (66.7)	10 (83.3)	0.392
Ethnic Group = Non-Hispanic or Non-Latino (%)	10 (83.3)	10 (83.3)	10 (83.3)	11 (91.7)	0.919
Hospitalized = YES (%)	12 (100.0)	12 (100.0)	12 (100.0)	12 (100.0)	NA
ICU Patient = NO (%)	12 (100.0)	12 (100.0)	12 (100.0)	12 (100.0)	NA
ICU Event = NO (%)	12 (100.0)	12 (100.0)	12 (100.0)	12 (100.0)	NA
Time difference sample collection to hospitalization / h	6.00 (20.78)	8.00 (18.68)	8.00 (21.30)	12.00 (19.15)	0.903
Lagtime / h	80.26 (17.83)	78.90 (15.77)	78.73 (27.19)	84.29 (11.88)	0.881
Glucose Level / mg/dL	174.60 (83.90)	111.50 (14.47)	151.64 (46.72)	105.78 (22.77)	0.019
CRP Inflammatory / mg/L	130.10 (100.63)	96.84 (137.65)	NaN (NA)	117.55 (103.45)	0.907
D Dimer / ug/mL	2.09 (1.36)	0.76 (0.40)	NaN (NA)	3.33 (NA)	NA
Ferritin Level / ng/mL	852.40 (597.04)	951.00 (1208.95)	NaN (NA)	98.00 (NA)	NA
International Normalized Ratio (INR) in Platelet Poor Plasma	1.61 (0.55)	1.11 (0.22)	1.31 (0.39)	1.15 (0.11)	0.481
Troponin T / ng/mL	0.01 (0.01)	0.00 (0.01)	0.72 (1.02)	0.00 (NA)	NA
Troponin T Interp (%)					0.497
GRAYZONE	1 (20.0)	0 (0.0)	0 (0.0)	0 (0.0)	
NEGATIVE	4 (80.0)	2 (100.0)	1 (50.0)	1 (100.0)	
POSITIVE	0 (0.0)	0 (0.0)	1 (50.0)	0 (0.0)	
CO2 level / mmol/L	23.30 (2.87)	24.50 (2.56)	24.09 (5.49)	23.33 (2.29)	0.876
ALT / units/L	21.25 (12.98)	31.40 (11.17)	29.00 (19.94)	37.33 (26.16)	0.499
AST / units/L	31.88 (18.54)	29.80 (6.53)	43.83 (22.16)	41.33 (30.17)	0.573
Albumin level / g/dL	3.18 (0.34)	3.46 (0.85)	3.13 (0.71)	3.57 (0.55)	0.653
Bilirubin Total / mg/dL	0.46 (0.35)	0.52 (0.22)	0.55 (0.44)	0.97 (1.00)	0.476
Creatinine level / mg/dL	2.43 (3.03)	1.01 (0.27)	1.99 (2.08)	0.85 (0.38)	0.244
BUN level / mg/dL	33.80 (27.37)	19.12 (17.36)	29.55 (22.40)	14.67 (10.06)	0.18
LD / units/L	321.33 (90.96)	372.00 (41.39)	NaN (NA)	297.50 (86.97)	0.549
Lactic Acid level / mmol/L	1.35 (0.33)	2.05 (0.64)	1.00 (0.28)	1.70 (0.71)	0.225
Calcium level / mg/dL	8.86 (0.42)	8.76 (0.51)	8.95 (0.64)	8.59 (0.37)	0.449
Chloride level / mmol/L	98.80 (6.56)	105.12 (8.56)	100.18 (4.79)	103.22 (6.40)	0.178
Potassium level / mmol/L	4.35 (0.54)	4.12 (0.30)	4.35 (0.44)	3.93 (0.39)	0.123
Sodium level / mmol/L	134.80 (5.14)	141.12 (9.01)	135.45 (4.46)	136.44 (5.94)	0.156
White Blood Cells	8.32 (3.86)	7.12 (3.24)	9.53 (2.18)	8.90 (2.11)	0.456
Abs Lymphocyte Count	0.93 (0.81)	0.95 (0.55)	1.87 (0.37)	1.72 (1.06)	0.078
Abs Basophil Count	0.04 (0.09)	0.02 (0.02)	0.03 (0.01)	0.03 (0.02)	0.889
Abs Eosinophil Count	0.03 (0.04)	0.06 (0.05)	0.37 (0.39)	0.20 (0.19)	0.03
Abs Monocyte Count	0.55 (0.64)	0.40 (0.16)	0.69 (0.08)	0.73 (0.28)	0.575
Abs Neutrophil Count	6.64 (2.99)	4.52 (2.80)	6.47 (1.69)	6.24 (1.98)	0.46
Lymphocytes (%)	13.61 (15.99)	18.52 (17.13)	20.50 (7.01)	19.80 (13.24)	0.82
Basophils (%)	0.48 (1.02)	0.30 (0.31)	0.38 (0.15)	0.30 (0.23)	0.955
Eosinophils (%)	0.34 (0.52)	0.95 (0.89)	3.82 (3.65)	2.40 (2.27)	0.033
Monocytes (%)	5.58 (3.20)	6.03 (1.85)	7.54 (1.87)	8.22 (3.40)	0.348
Neutrophils (%)	77.56 (18.11)	63.53 (23.55)	67.58 (9.11)	69.10 (17.44)	0.54

Data presented as Mean (Standard Deviation) unless otherwise specified. NA: not applicable, NaN: not a number.

expression analysis are reported in Supplementary Tables ST4-ST6. As shown in Fig. 2A,C and Fig. 3A,C, the multidimensional scaling (MDS) plots of all EV proteomic and EV phosphoproteomic data passing stringent filtering criteria and the unsupervised clustering of the respective differentially expressed EV signatures effectively distinguished the four study groups. Only one patient with COVID-19 and T2D was misclustered with the RSP+ T2D- group by unsupervised clustering of DE proteins, however, its specific DE proteomic signature was clearly distinct from that of the real RSP+ T2D- patients. Of note, the distance attributable to T2D in the MDS plots is greater in RSP+ patients compared to COVID-19 ones (Fig. 2C and 3C). The volcano plots shown in Fig. 2D,E and Fig. 3D,E highlight many of the differential expressed proteins and phosphosites that account for the independent effects of COVID-19 and T2D.

Additionally, Fig. 2B, 3B, and 4, as well as select boxplots presented in Supplementary Figures SF2 and SF3, highlight the EV proteins and phosphoproteins that are significantly changed in multiple comparisons. Notably, coagulation Factor VIII (F8, Fig. 4, Supplementary Figure SF4A,F) was found to be a unique feature that significantly changed due to both COVID-19 and T2D at both the protein and phosphoprotein level (Fig. 4B), and further displayed an interaction effect between the two diseases (Fig. 3B and 4A). Similar to protein F8, integrin ITGA6, HSP90AB1, and LIMS1 were three additional DE phosphoproteins that demonstrated significant COVID-19 by T2D interaction effect at the protein level (Fig. 4A,B, Supplementary Figure SF4B-D,G-I). MAP2K2 was another relevant DE phosphoprotein with significant COVID-19 and T2D independent effects (Fig. 4B, Supplementary Figure SF4E). Interestingly, most of the above-mentioned DE phosphoproteins appeared to be coregulated, as demonstrated by the significant correlations among their circulating EV levels (Supplementary Figure SF5). The important role of MAPK signaling for integrin signaling is further highlighted by the Reactome pathway enrichment analysis among differentially expressed phosphoproteins shown in Supplementary Figure SF4J.

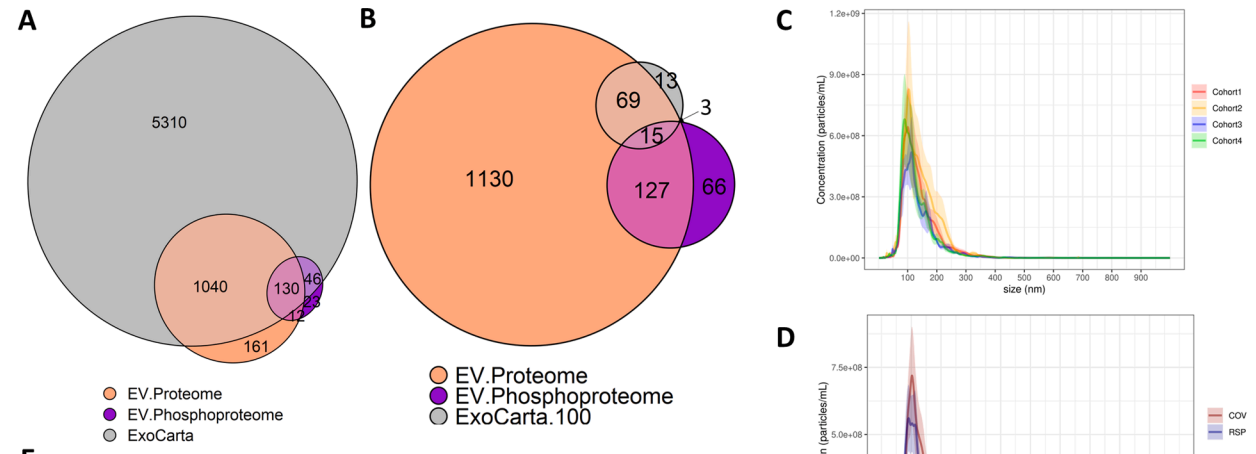

E

Group	Total Conc. Mean (particles/mL)	Total Conc. Median (particles/mL)	Size Mode (nm)	Size Mean (nm)	Mean SD (nm)	Size D10 (nm)	Size D50 (nm)	Size D90 (nm)
COV+T2D+	5.92E+10	4.18E+10	103	134	54.8	82.4	122	206
COV+T2D-	7.05E+10	2.88E+10	110	141	53.0	88.8	130	208
RSP+T2D+	4.49E+10	4.23E+10	109	135	55.2	82.0	123	202
RSP+T2D-	5.30E+10	3.96E+10	105	132	53.7	81.5	118	200

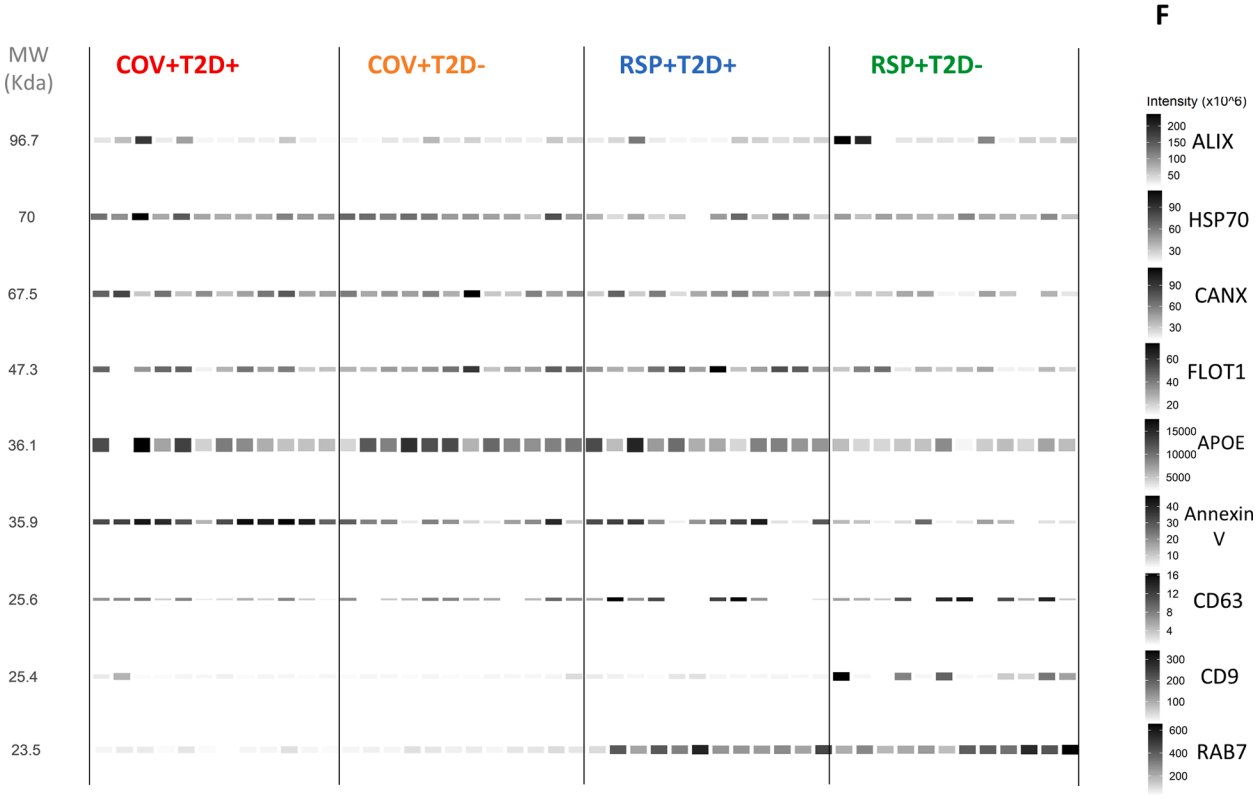

Fig. 1. Proteomic signatures of circulating EVs in hospitalized patients with either COVID-19 or alternative acute respiratory disease (RSP), with or without T2D. (A, B) Comparison of detected EV proteins and reported exosomal proteins in full (A) and top 100 (B) Exocarta database. (C,D) Particle distributions as determined by nanoparticle tracking analysis of EV preparations from each study cohorts (C) and summarized by COVID-19 or RSP diagnosis (D). (E) Summary statistics from the NTA analysis. (F) Digital Western-like rendering of proteomic data for classical EV markers.

3.3.1. Dual phosphoprotein- and phosphosite-centric analysis uncovered unique signatures of upstream PKC, MAPK, AMPK, and SYK activation

Using *directPA* (an R package that can integrate multiple treatments and visualize kinases and substrates under combinatorial perturbations [32]), we predicted upstream activated kinases presumably responsible for the observed phosphopeptide profiles in the circulating EVs (Fig. 5A). Most notably, the kinase perturbation analysis predicted reduced PKC activity (marked by PRKCA, one of the protein kinase C family members) in both COVID-19 and T2D conditions, and reduced MAPK activity in COVID-19 (Fig. 5A). On the other hand, AMPK (marked by the catalytic subunit PRKACA) activation was predicted in COVID-19 and contrasted by reduced activity in T2D (Fig. 5A). Supporting these predictions, PKC family member PRKCB (PKCβ) was found to be significantly downregulated at the protein level in both COVID-19

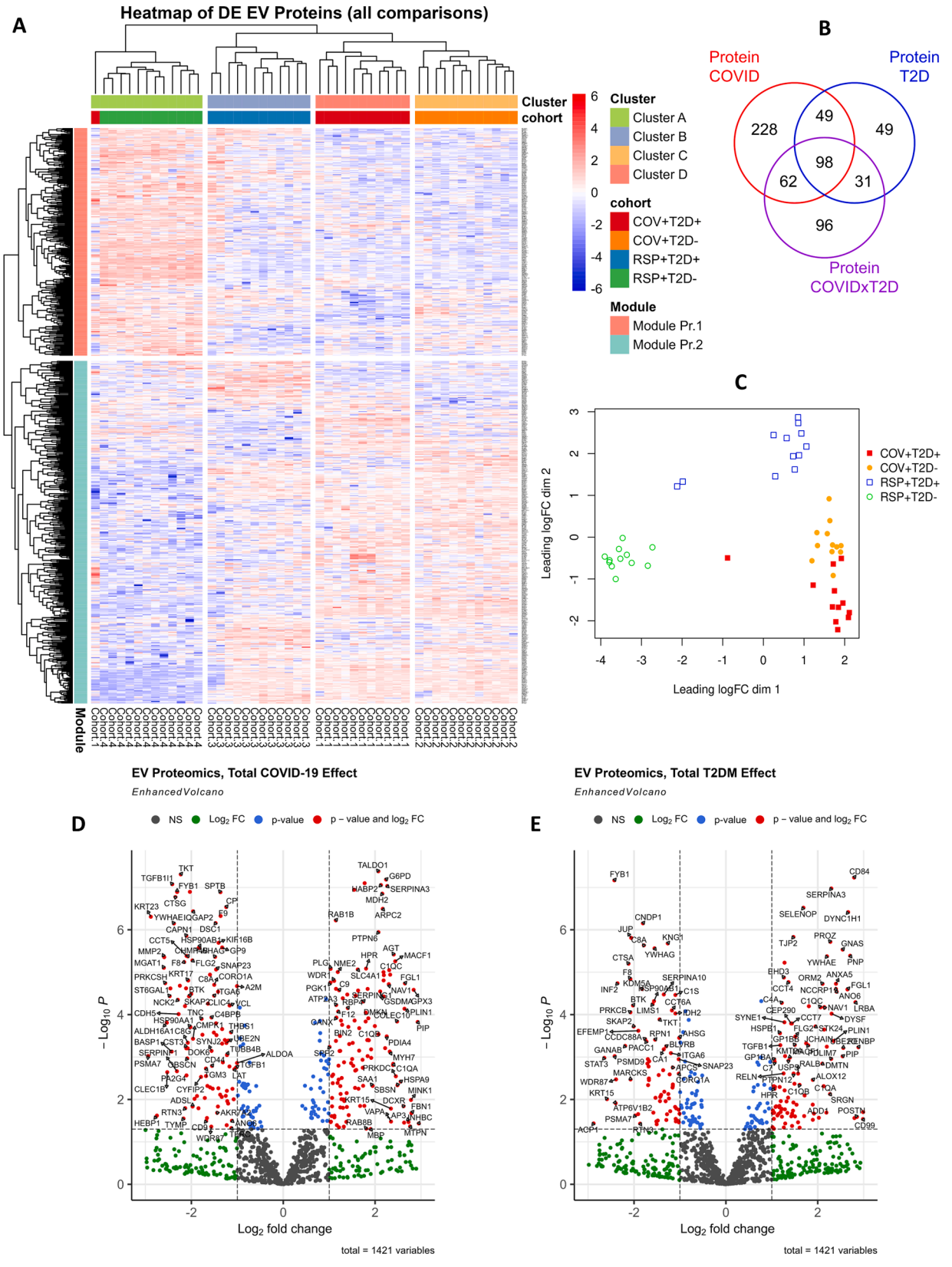

Fig. 2. Global EV proteomics signatures. (A) Unsupervised hierarchical clustering of differentially expressed EV proteins. (B) Cross-referencing of differentially expressed EV proteins defining the main independent effects of COVID-19 and T2D, and the corresponding disease interaction effect. (C) Multidimensional scaling plot of Euclidean distances among groups based on the normalized abundance levels of all detected EV proteins. (D,E) Volcano plots highlighting differentially expressed EV proteins defining the independent effects of COVID-19 and T2D.

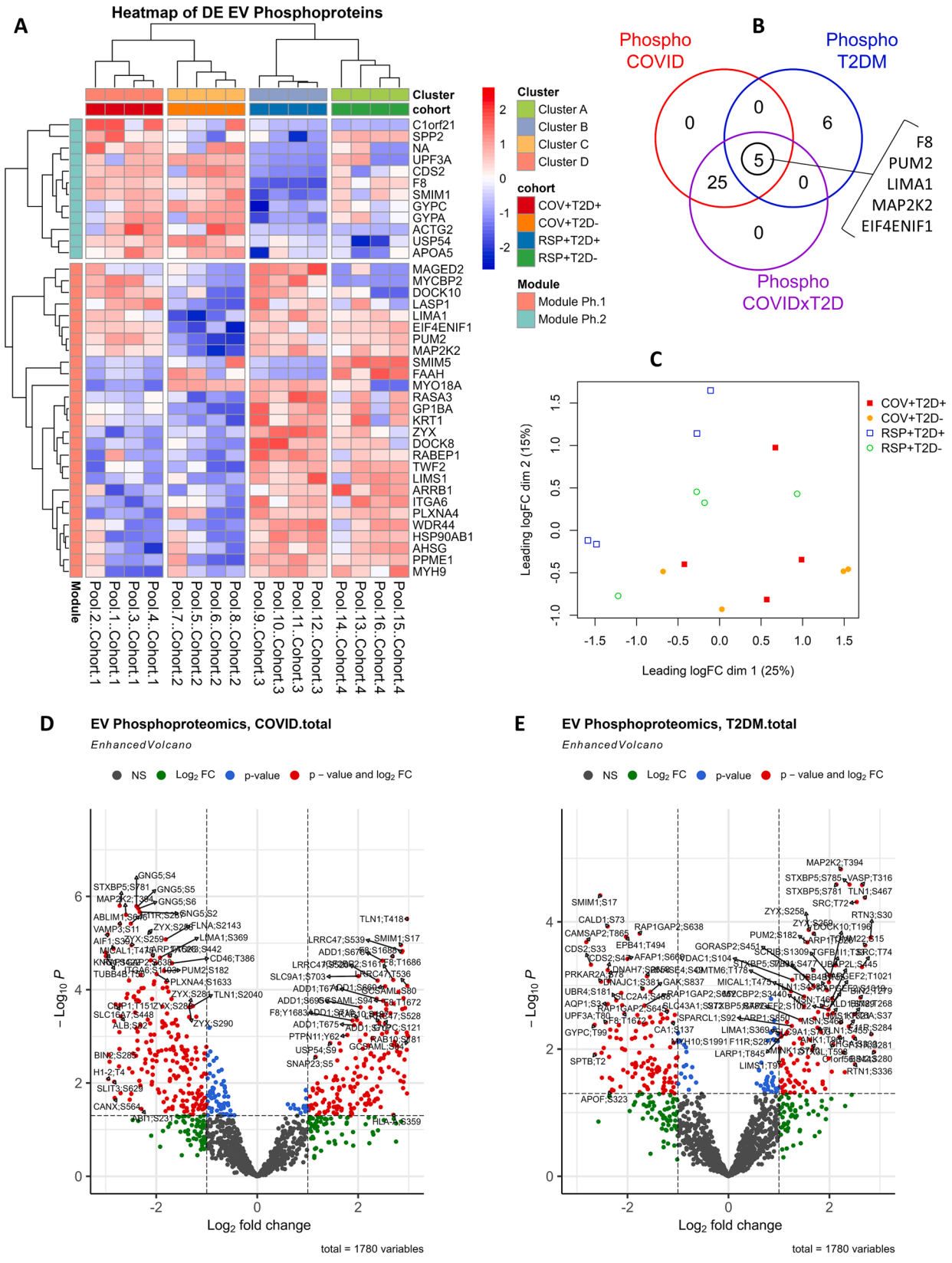

Fig. 3. Global EV phosphoproteomics signatures. (A) Unsupervised hierarchical clustering of differentially expressed EV phosphoproteins. (B) Cross-referencing of differentially expressed EV phosphoproteins defining the main independent effects of COVID-19 and T2D, and the corresponding disease interaction effect. (C) Multidimensional scaling plot of Euclidean distances among groups based on the normalized abundance levels of all detected EV phosphoproteins. (D,E) Volcano plots highlighting differentially expressed EV phosphosites defining the independent effects of COVID-19 and T2D.

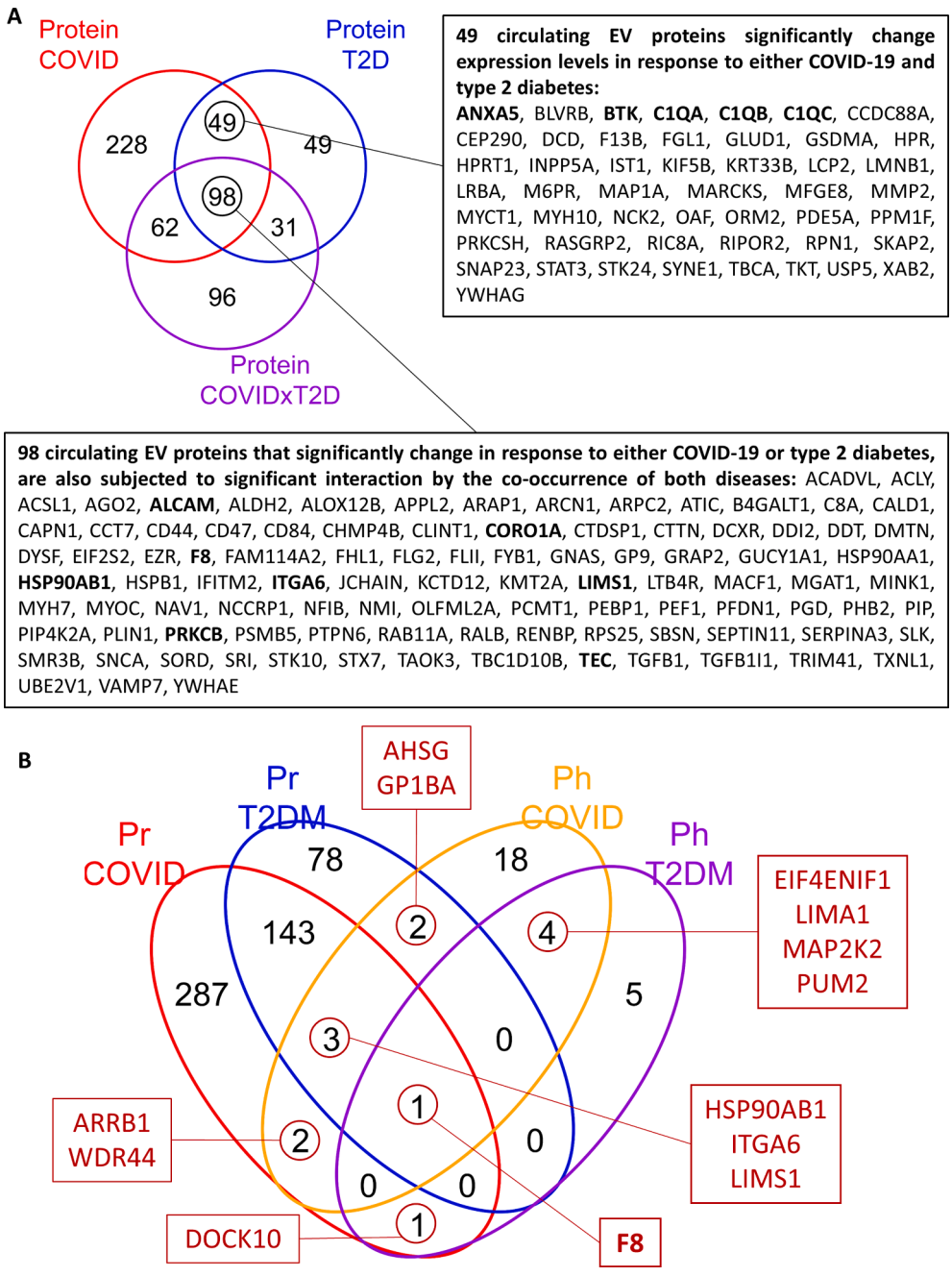

Fig. 4. Cross-referencing of differentially expressed EV proteins and EV phosphoproteins. (A) Venn diagram highlighting the common EV proteomic signatures among the main independent effects of COVID-19 and T2D, and the corresponding disease interaction effect. (B) Venn diagram highlighting the common EV proteomic and phosphoproteomic signatures characterizing the main independent effects of COVID-19 and T2D.

and T2D patients, and to be additionally subjected to significant interaction effect between the two diseases (Fig. 4A, Supplementary Figures SF2D). In addition, protein PRKAR2B (the key AMPK regulatory subunit involved in adipose tissue development [34]) (Supplementary Figure SF2E) and phosphorylated MAP2K2 (Supplementary Figure SF4E) were found to be significantly downregulated in EVs from COVID-19 patients. In addition, using package *PhosR* [29,30], we identified potential kinase-substrate pairs (Fig. 5B, row dendrogram) and global relationships between kinases (Fig. 5B, column dendrogram). *PhosR* was also used to construct signalomes that report on protein modules with phosphosites that share similar dynamic phosphorylation profiles and kinase regulation (Fig. 5C). These signalomes revealed that several phosphosite modules were exclusively regulated by SYK or MAP3K7, while the rest seemed coregulated by multiple kinases, suggesting potential signaling crosstalk and/or redundancy.

3.3.2. Functional enrichment among differentially expressed EV proteins suggest additional clinically relevant COVID-19 - T2D relationships

To gain additional insight into mechanisms driving the increased risk for hospitalization with COVID-19 among people with T2D, we constructed networks of enriched KEGG pathways among the differentially abundant EV proteins (Supplementary Figure SF6, Supplementary Tables ST7-ST12). We detected common functional node clusters among the networks assessing the independent effects of COVID-19 and T2D. A key central cluster appeared to be the significantly upregulated trio of adaptive immune response complement proteins C1QA, C1QB, and C1QC in EVs (Fig. 4A, Supplementary Figure SF2A-C, SF6B,D).

Also common between the independent effects of COVID-19 and T2D

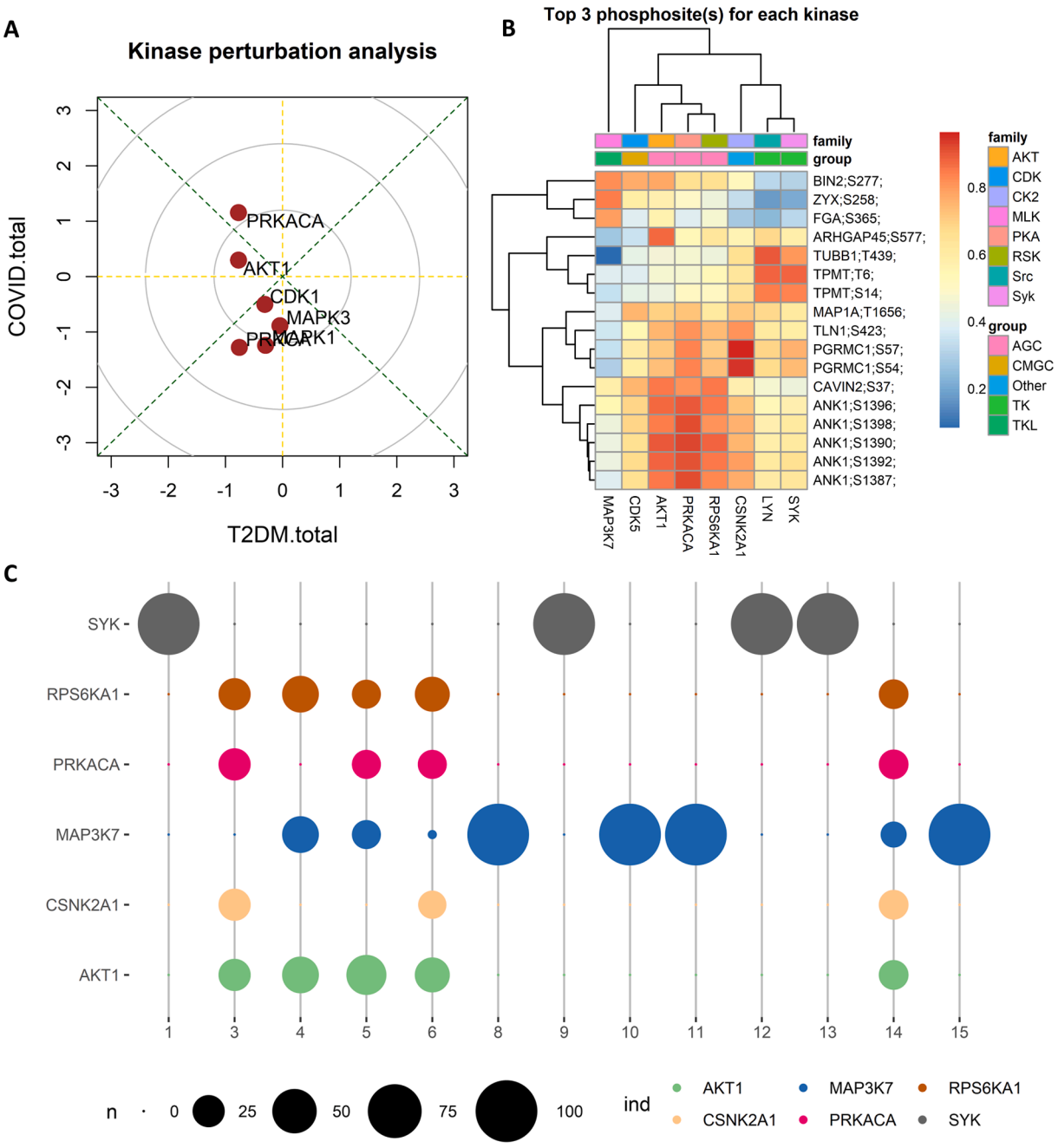

Fig. 5. Global kinase activity prediction analyses. (A) Kinase perturbation analysis based on the differentially expressed EV phosphopeptide profiles defining the independent effects of COVID-19 and T2D. (B) Heatmap of global kinase-substrate relationships scores for the top three EV phosphosites of all evaluated kinases. The higher the scores, the better the fit of a phosphosite to a kinase motif and kinase-substrate EV phosphorylation profile. Kinases are annotated by kinase family and group. (C) EV signalomes for kinases with predicted substrates. Solid circles represent the protein modules regulated by each predicted kinase. Circle size is proportional to the number of proteins predicted to be regulated by the specific kinases. Only significantly upregulated phosphosites were included in the analysis.

was the significant downregulation of PRKCB (mentioned in previous section, Fig. 4A, Supplementary Figures SF2D and SF6A,C,F). In addition, protein levels of BTK and TEC (two TEC kinase family members), were also significantly downregulated in EVs from both patients with COVID-19 or T2D (logFC < -2, FDR≪<≪0.05, Supplementary Table ST1-ST2, Supplementary Figure SF2F,G). Significant correlations ($r \geq 0.63$, P<<0.05) were detected among the three EV kinases PRKCB, BTK, and TEC (Supplementary Figure SF2J-L) that suggested their co-regulation in COVID-19 and T2D. PRKCB and TEC additionally displayed significant COVID-19 by T2D interaction (Fig. 4A).

Moreover, we observed that upregulation of EV CASP3 was central in COVID-19-specific networks (Supplementary Table ST1, Supplementary Figures SF2H and SF6B). On the other hand, Rho kinase (ROCK1) was one of the most strongly downregulated proteins in COVID-19 patients (Supplementary Table ST1, Supplementary Figures SF2I and SF6A) and the levels of EV ROCK1 were negatively correlated with the levels of EV CASP3 ($r = -0.7$, $P = 2.6 \times 10^{-6}$, Supplementary Figure SF3D). These two proteins additionally display significant COVID-19 by T2D interaction effects (Supplementary Table ST3, Supplementary Figure SF6E, F).

We further detected highly significant COVID-19 - T2D interaction effects in the trafficking molecule ALCAM (Supplementary Tables ST1-ST3, Supplementary Figures SF2J and SF6F) and lysosome-resident LAMP1 (Supplementary Tables ST1 and ST3, Supplementary Figures

SF2K and SF6A,F). Another set of interesting lysosome- and autolysosome-related proteins that demonstrated differential expression in the circulating EVs were VAMP8, ATP6V1A, ATP6V1B2 and ATP6V1H (Supplementary Tables ST1-ST3, Supplementary Figures SF2L-O and SF6A,F). Other molecules involved in phagosome function including RAB5B, CORO1A, FCGR3B, and CD36 (Supplementary Table ST3, Supplementary Figures SF2P-R and SF6F) also became significantly elevated in the circulating EVs from patients with concomitant COVID-19 and T2D.

4. Discussion

The large amount of information generated by multiomic studies makes the integrated evaluation and comprehensive interpretation of the results challenging. Here, we focused our discussion on the most relevant findings that, supported by recent published literature, underscored the novel contribution of circulating EVs to the increased risk for hospitalization in COVID-19 patients with T2D.

EV preparations were highly enriched in exosomal proteins, demonstrating that approximately 86% of all detected proteins are annotated as EV proteins by the Exocarta database, including 87 of the proteins considered to be the best exosomal markers (Top 100 Exocarta list). Although we observed increased particle concentration for the COVID-19 groups, as compared to their respective non-COVID-19 controls, across most of the analyzed size range, the increased was not significant. Interestingly, some classical exosomal markers such as Annexin-V and RAB7 (albeit in opposite directions), as well as some presumably contaminating proteins such as Calnexin showed significantly deregulated levels in circulating EVs from the COVID-19 groups. Because the method we employed for EV purification has been demonstrated to produce highly enriched EV preparations, we reasoned that the presence of specific proteins generally considered to be contaminating proteins may underlie relevant biological changes of EV composition and/or EV corona, induced by COVID-19 and possibly viral infections in general [35–37]. However, as a limitation of our study, we are not able to confirm this because we do not have a comparable control group exempted of viral infection. On the other hand, because RAB7 regulates the secretion of exosomes, dependent on cell type, by promoting fusion of the multivesicular bodies with the lysosome [38], we reason that the downregulation of RAB7 due to COVID-19 in our study patients may contribute to the release of intralumenal vesicles (that would have been otherwise detoured for lysosomal degradation/recycling) as exosomes. This reasoning is supported by a recent report by Wei and colleagues [39].

Among additional relevant findings, the fact that the distance attributable to T2D in the MDS plots (Fig. 2B and 3B) is greater among the RSP groups compared to COVID-19 ones, suggested that, different from non-COVID acute respiratory diseases, COVID-19 and T2D must be similarly regulated by or alter a number of key cellular pathways that makes the molecular fingerprint of the two diseases somewhat similar. Supporting this reasoning, the upregulation of the C1QA, C1QB, and C1QC trio of proteins in the circulating plasma EVs, due to both independent effects of COVID-19 and T2D, suggests that $C1Q^{+}$ EVs may contribute to the spread of immuno-modulatory and prothrombotic cargo, and consequently, to generalized organ damage [40,41] in both diseases. The C1Q proteins are predominantly produced by antigen presenting cells such as monocytes, macrophages, and dendritic cells [42]. These proteins have been reported to transiently attach to the cell surface, during which time, they can recognize danger signals via their antigen-binding globular head domains [42]. In similar fashion to TNFα, locally synthesized C1Q can induce immunomodulatory effects via autocrine and/or paracrine signaling [42]. Therefore, we reason that the presence of the C1Q proteins on the EV surface may reflect an increased production of these molecules by a variety of activated antigen presenting cells (APC) in response to SARS-CoV-2 infection and/or diabetes. On the other hand, the $C1Q^{+}$ EVs may themselves spread immuno-modulatory cargo away from the localized sites of APC infiltration and C1Q synthesis. This may extend the immunological paradigm "local synthesis for local function" [42,43] into a "local synthesis for local and systemic function" paradigm. Interestingly, Factor VIII (F8, FVIII), another procoagulant factor that is stored in endothelial cells and released during inflammation, was detected in both our COVID-19 and T2D effect networks and found to be significantly downregulated in the circulating EVs at the protein level but upregulated in the phosphorylated state. Supporting the role of FVIII in severe COVID-19, Tabatabai and colleagues reported the significant elevation of circulating F8 in critically ill COVID-19 patients [44]. Similarly, Rauch and collaborators reported the progressive elevation of FVIII blood levels in COVID-19 (out-, ward, and intensive care unit) patients [45].

The significant downregulation of PRKCB (PKCβ) at the protein level, due to both the independent effects of COVID-19 and T2D, is also relevant and supports our kinase perturbation analysis results suggesting upstream activation of a PKC family member. Notably, PKC activity was found to increase within 15 min of SARS-CoV-2 infection and to contribute (particularly PKCβ) to viral entry into the host cell [46]. Our results suggest that SARS-CoV-2 infection may alter the cellular secretory pathway to retain PKCβ, consequently increasing its intracellular activity while reducing its concentration (and possibly its activity) in secreted exosomes. PKCβ was also reported to negatively regulate the B-cell receptor signalosome by downregulating BTK activity via alteration of BTK plasma membrane localization in human and mouse cell cultures [47]. PKC and BTK were also found to be involved in IFN-β production triggered by TLR7/9 in conventional dendritic cells [48]. Of note, the significant correlations demonstrated in our study among the three EV kinases, namely PRKCB, BTK, and TEC, further underscores the role of a coregulated PKC/BTK/TEC axis in COVID-19 and T2D. We reason that, by impairing the humoral immune response via downregulation of BTK/TEC kinase activity, increased PKCβ in immune cells could contribute to enhanced SARS-CoV-2 escape, particularly in patients with T2D. These findings suggest therapeutic utility for PKC inhibitors against COVID-19 in humans with and without T2D. In particular, the pan-PKC inhibitor bisindolylmaleimide-IX seems promising as it was additionally demonstrated, by virtual screening and in vitro validation assays, to target the main SARS-CoV-2 protease 3CLpro [49] Importantly, similar to our study, another proteomic and phosphoproteomic study of COVID-19 in macaques identified members of the PKC and AMPK families activated in the liver, where these kinases play key metabolic roles [50]. These authors also found proliferation-related MAP2K2 to be activated in infected macaque lungs and drug enrichment analysis suggested that fostamatinib, an inhibitor of SYK used to treat thrombocytopenia, could be an effective drug against the activated kinases detected in both the lungs and liver [50]. Our phosphoproteomics analysis also suggested important roles for MAP2K2 and SYK kinases. Remarkably, the SYK inhibitor fostamatinib was recently reported to produce improved clinical outcomes in hospitalized patients with COVID-19 [51].

A central role for EV-shuttled CASP3 is suggested by the COVID-19-specific network. Supporting our findings, Moon and colleagues reported that large amount of EVs loaded with CASP3 were produced by lung epithelial cells and released into the bronchoalveolar lavage fluid (BALF) of a hyperoxia mouse model [52]. These EVs induced a potent inflammatory response in alveolar macrophages via activation of the ROCK1 pathway [52]. In addition to a burst in inflammatory insults, activation of ROCK1 promotes immune cell migration, apoptosis, coagulation, and cell adhesion in pulmonary endothelial cells that disrupt the endothelium barrier and causes edema and lung injury [53]. Because our patients with COVID-19 and T2D not only maintained elevated levels of EV-shuttled CASP3 but also increased levels of EV-shuttled ROCK1 (compared to COVID-19 patients without T2D), we speculate that the EV-shuttled CASP3-ROCK1 pair may promote the activation of macrophages in distant tissues, even if the basal expression of ROCK1 in such distant tissues was relatively low. Notably, inhibitors of ROCK1 (i.e., isoquinoline derivative fasudil) were suggested to have

utility in the treatment of COVID-19 [53–55]. Our clinically relevant data adds support to ROCK1 inhibition as therapeutic option in patients with COVID-19, particularly those with concurrent T2D. Fasudil has been approved in Japan since 1995 for the treatment of vasospasms following subarachnoid hemorrhage and it is known to have a favorable side effect profile in those patients and in patients with cardiovascular disease [56] and amyotrophic lateral sclerosis [57]. Those characteristics may facilitate the repurposing of Fasudil as a COVID-19 therapeutic option.

The highly significant COVID-19 - T2D interaction detected in trafficking molecule ALCAM is supported by the observations of Larochelle et al., who demonstrated that elevated proportions of $ALCAM^{+}$ monocytes are specifically associated with SARS-CoV-2 infection in hospitalized patients and correlated with disease severity and mortality [58]. Because ALCAM is involved in leukocyte transendothelial migration (one of the KEGG pathways found enriched among the differentially expressed EV proteins identified in our study) and the stabilization of the immune synapse [58,59], we reasoned that its highly elevated levels in circulating EVs from COVID-19 patients with T2D may indicate an enhanced EV-mediated communication activity among immune cells and the endothelium, which would consequently contribute to the increased inflammatory milieu in these patients. Adding to Larochelle's group findings, our results now suggest that EVs may play a central communication role contributing to the severity of COVID-19 disease.

Other results, in particular, the significant differential expression of LAMP1, VAMP8, ATP6V1A, ATP6V1B2, ATP6V1H, RAB5B, CORO1A, FCGR3B, and CD36, further demonstrated that the lysosome and autolysosome functions appear to also play an important role driving the COVID-19 - T2D interaction. Supporting our observations, Miao and collaborators recently demonstrated that the ORF3a protein of the SARS-CoV-2 virus localizes to the late-endosome and blocks autophagosome and amphisome fusion with lysosomes by blocking the assembly of the STX17-SNAP29-VAMP8 SNARE complex, which allows the virus to escape lysosomal destruction.[60] The significant COVID-19 effect (downregulation) observed on the EV-shuttled VAMP8 levels in our study is consistent with the reported blockage of SNARE complexes in SARS-CoV-2 infected cells [60]. On the other hand, the significant reduction of ATP6V1A, ATP6V1B2 and ATP6V1H subunits of the vacuolar ATPase (V-ATPase), which mediates acidification of membrane-bound compartments such as lysosomes, endosomes, and secretory granules, is strongly consistent with the report by the Altan-Bonnet group [61]. These authors showed that β-coronaviruses including SARS-CoV-2 associate with the lysosomes and/or atypical late endosomes in infected cells, consequently reducing the lysosome acidity, inactivating lysosomal degradation enzymes, and disrupting the antigen presentation pathways before egressing via lysosomal exocytosis [61]. On the other hand, LAMP1, another lysosome-resident protein, was previously demonstrated to function as an intracellular receptor for the Lassa virus, which allows the virus to switch receptors when the pH change is sensed [62,63]. Interestingly, LAMP1 was significantly downregulated in the circulating EVs of our COVID-19 patients without T2D but significantly upregulated by the interaction between COVID-19 and T2D. We reason that this increased in LAMP1 abundance while the levels of VAMP8 and the V-ATPase subunits are maintained or significantly reduced (as compared to the COVID-19 patients without diabetes) suggests that in patients with COVID-19 and T2D, the SARS-CoV-2 virus may more readily transit and egress via the lysosomes, likely and consequently displaying more efficient infectivity that may contribute to the increased severity of the disease in these patients. These results suggest that targeting of the SARS-CoV-2 protein ORF3a might be a particularly effective therapeutic strategy in this patient subgroup with concomitant COVID-19 and T2D.

In conclusion, this study characterized the circulating EV proteomic and phosphoproteomic landscapes of COVID-19 and alternative non-COVID-19 acute respiratory disease in the context of comorbid type 2 diabetes, and suggested potential functional mechanisms that may contribute to the increased risk for hospitalization in this patient population. Additionally, these results suggest potential druggable targets and therapeutic strategies that may be beneficial to these patients. Although the study is limited by a relatively small sample size, the careful selection of the study cohorts, the representation of multiple races and ethnicities, and the use of state-of-the-art methods for non-antibody-based specific EV isolation strengthen and suggest generalizability of our results. Another limitation is that we had access to only a small volume of plasma per sample, which required a pooling strategy to produce insights into the EV phosphoproteomic landscape and kinase signaling in our study population. For these reasons, further validation on independent COVID-19 and T2D cohorts is needed. Future studies should also address the characterization of circulating EVs in prospective longitudinal studies to assess whether the COVID-19 by T2D interaction signatures identified in this study contribute to the development and/or progression of severe COVID-19 and mortality.

Disclosure summary

This study was funded by program funds granted to REP by the AdventHealth Translational Research Institute. REP reports grants from Hanmi Pharmaceutical Co.; grants from Janssen; consulting fees from Merck; grants, speaker fees and consulting fees from Novo Nordisk; consulting fees from Pfizer; grants from Poxel SA; grants and consulting fees from Sanofi; consulting fees from Scohia Pharma Inc.; consulting fees from Sun Pharmaceutical Industries. AI is a principal at Tymora Analytical Operations, which developed the EVtrap™ beads. AC reports consulting fees from GlaxoSmithKline. Honoraria and fees for REP's and AC's services were paid directly to AdventHealth, a nonprofit organization. No other potential conflicts of interest relevant to this article were reported.

Funding

This research was funded by program funds granted to REP by the AdventHealth Translational Research Institute.

Declaration of Competing Interest

The authors declare that they have no known competing financial interests or personal relationships that could have appeared to influence the work reported in this paper.

Appendix A. Supplementary material

Supplementary data to this article can be found online at https://doi.org/10.1016/j.diabres.2023.110565.

References

[1] Turk Wensveen T, Gašparini D, Rahelić D, Wensveen FM. Type 2 diabetes and viral infection; cause and effect of disease. Diabetes Res Clin Pract 2021;172.
[2] Ceriello A, De Nigris V, Prattichizzo F. Why is hyperglycaemia worsening COVID-19 and its prognosis? Diabetes Obes Metab 2020.
[3] Nunez Lopez YO, Casu A, Pratley RE. Investigation of Extracellular Vesicles From SARS-CoV-2 Infected Specimens: A Safety Perspective. Front Immunol 2021:12.
[4] Zaid Y, Puhm F, Allaeys I, Naya A, Oudghiri M, Khalki L, et al. Platelets Can Associate with SARS-Cov-2 RNA and Are Hyperactivated in COVID-19. Circ Res 2020.
[5] Cappellano G, Raineri D, Rolla R, Giordano M, Puricelli C, Vilardo B, et al. Circulating Platelet-Derived Extracellular Vesicles Are a Hallmark of Sars-Cov-2 Infection. Cells 2021:10.
[6] Barberis E, Vanella VV, Falasca M, Caneapero V, Cappellano G, Raineri D, et al. Circulating Exosomes Are Strongly Involved in SARS-CoV-2 Infection. Front Mol Biosci 2021;8:632290.
[7] Krishnamachary B, Cook C, Spikes L, Chalise P, Dhillon NK. The Potential Role of Extracellular Vesicles in COVID-19 Associated Endothelial injury and Pro-inflammation. medRxiv. 2020.
[8] Tertel T, Tomić S, Đokić J, Radojević D, Stevanović D, Ilić N, et al. Serum-derived extracellular vesicles: Novel biomarkers reflecting the disease severity of COVID-19 patients. J Extracellular Vesicles 2022;11:e12257.

[9] Fu B, Wang D, Shen X, Guo C, Liu Y, Ye Y, et al. Immunomodulation Induced During Interferon-α Therapy Impairs the Anti-HBV Immune Response Through CD24(+)CD38(hi) B Cells. Front Immunol 2020;11:591269.

[10] Newell KL, Clemmer DC, Cox JB, Kayode YI, Zoccoli-Rodriguez V, Taylor HE, et al. Switched and unswitched memory B cells detected during SARS-CoV-2 convalescence correlate with limited symptom duration. PLoS One 2021;16: e0244855.

[11] Lakhter AJ, Sims EK. Minireview: Emerging Roles for Extracellular Vesicles in Diabetes and Related Metabolic Disorders. Mol Endocrinol 2015;29:1535–48.

[12] Gao X, Salomon C, Freeman DJ. Extracellular Vesicles from Adipose Tissue-A Potential Role in Obesity and Type 2 Diabetes? Front Endocrinol (Lausanne) 2017; 8:202.

[13] Prabu P, Rome S, Sathishkumar C, Gastebois C, Meugnier E, Mohan V, et al. MicroRNAs from urinary extracellular vesicles are non-invasive early biomarkers of diabetic nephropathy in type 2 diabetes patients with the 'Asian Indian phenotype'. Diabetes Metab 2019;45:276–85.

[14] Noren Hooten N, Evans MK. Extracellular vesicles as signaling mediators in type 2 diabetes mellitus. Am J Physiol Cell Physiol 2020;318:C1189–99.

[15] Wu SF, Noren Hooten N, Freeman DW, Mode NA, Zonderman AB, Evans MK. Extracellular vesicles in diabetes mellitus induce alterations in endothelial cell morphology and migration. J Transl Med 2020;18:230.

[16] Prattichizzo F, De Nigris V, Sabbatinelli J, Giuliani A, Castaño C, Párrizas M, et al. CD31(+) Extracellular Vesicles From Patients With Type 2 Diabetes Shuttle a miRNA Signature Associated With Cardiovascular Complications. Diabetes 2021; 70:240–54.

[17] Prattichizzo F, Matacchione G, Giuliani A, Sabbatinelli J, Olivieri F, de Candia P, et al. Extracellular vesicle-shuttled miRNAs: a critical appraisal of their potential as nano-diagnostics and nano-therapeutics in type 2 diabetes mellitus and its cardiovascular complications. Theranostics 2021;11:1031–45.

[18] Nunez Lopez YO, Casu A, Kovacova Z, Petrilli AM, Sideleva O, Tharp WG, et al. Coordinated regulation of gene expression and microRNA changes in adipose tissue and circulating extracellular vesicles in response to pioglitazone treatment in humans with type 2 diabetes. Front Endocrinol (Lausanne) 2022;13:955593.

[19] Nunez Lopez YO, Iliuk A, Petrilli AM, Glass C, Casu A, Pratley RE. Proteomics and Phosphoproteomics of Circulating Extracellular Vesicles Provide New Insights into Diabetes Pathobiology. Int J Mol Sci 2022;23.

[20] Wu X, Li L, Iliuk A, Tao WA. Highly Efficient Phosphoproteome Capture and Analysis from Urinary Extracellular Vesicles. J Proteome Res 2018;17:3308–16.

[21] Iliuk A, Wu X, Li L, Sun J, Hadisurya M, Boris RS, et al. Plasma-Derived Extracellular Vesicle Phosphoproteomics through Chemical Affinity Purification. J Proteome Res 2020;19:2563–74.

[22] Zhang H, Deng Y, Liu X, Sun J, Ma L, Ding Y, et al. Glass Fiber-Supported Hybrid Monolithic Spin Tip for Enrichment of Phosphopeptides from Urinary Extracellular Vesicles. Anal Chem 2020;92:14790–7.

[23] Iliuk AB. Purification and Phosphoproteomic Analysis of Plasma-Derived Extracellular Vesicles. Methods Mol Biol 2022;2504:147–56.

[24] Willard NK, Salazar E, Oyervides FA, Wiebe CS, Ocheltree JS, Cortez M, et al. Proteomic Identification and Quantification of Snake Venom Biomarkers in Venom and Plasma Extracellular Vesicles. Toxins (Basel) 2021:13.

[25] Zhang H, Cai YH, Ding Y, Zhang G, Liu Y, Sun J, et al. Proteomics, Phosphoproteomics and Mirna Analysis of Circulating Extracellular Vesicles through Automated and High-Throughput Isolation. Cells 2022:11.

[26] Charles Jacob HK, Signorelli R, Charles Richard JL, Kashuv T, Lavania S, Middleton A, et al. Identification of novel early pancreatic cancer biomarkers KIF5B and SFRP2 from "first contact" interactions in the tumor microenvironment. J Exp Clin Cancer Res 2022;41:258.

[27] Abou Zeid F, Charrier H, Beseme O, Michel JB, Mulder P, Amouyel P, et al. Lim Domain Binding 3 (Ldb3) Identified as a Potential Marker of Cardiac Extracellular Vesicles. Int J Mol Sci 2022;23.

[28] Casu A, Lopez YON, Yu G, Clifford C, Bilal A, Petrilli AM, et al. Correlates of circulating extracellular vesicle cargo with key clinical features of type 1 diabetes. medRxiv. 2022:2022.03.10.22272207.

[29] Kim HJ, Kim T, Xiao D, Yang P. Protocol for the processing and downstream analysis of phosphoproteomic data with PhosR. STAR Protoc 2021;2:100585.

[30] Kim HJ, Kim T, Hoffman NJ, Xiao D, James DE, Humphrey SJ, et al. PhosR enables processing and functional analysis of phosphoproteomic data. Cell Rep 2021;34: 108771.

[31] Smyth GK. Linear Models and Empirical Bayes Methods for Assessing Differential Expression in Microarray Experiments. Stat Appl Genet Mol Biol 2004;3.

[32] Yang P, Patrick E, Humphrey SJ, Ghazanfar S, James DE, Jothi R, et al. KinasePA: Phosphoproteomics data annotation using hypothesis driven kinase perturbation analysis. Proteomics 2016;16:1868–71.

[33] Wu T, Hu E, Xu S, Chen M, Guo P, Dai Z, et al. clusterProfiler 4.0: A universal enrichment tool for interpreting omics data. Innovation (Camb) 2021;2:100141.

[34] Peverelli E, Ermetici F, Corbetta S, Gozzini E, Avagliano L, Zappa MA, et al. PKA regulatory subunit R2B is required for murine and human adipocyte differentiation. Endocr Connect 2013;2:196–207.

[35] Bridge SH, Pagano S, Jones M, Foster GR, Neely D, Vuilleumier N, et al. Autoantibody to apolipoprotein A-1 in hepatitis C virus infection: a role in atherosclerosis? Hepatol Int 2018;12:17–25.

[36] Kowalska K, Sabatowska Z, Forycka J, Mlynarska E, Franczyk B, Rysz J. The Influence of SARS-CoV-2 Infection on Lipid Metabolism-The Potential Use of Lipid-Lowering Agents in COVID-19 Management. Biomedicines 2022;10:2320.

[37] Fukushi M, Yoshinaka Y, Matsuoka Y, Hatakeyama S, Ishizaka Y, Kirikae T, et al. Monitoring of S protein maturation in the endoplasmic reticulum by calnexin is important for the infectivity of severe acute respiratory syndrome coronavirus. J Virol 2012;86:11745–53.

[38] Vanlandingham PA, Ceresa BP. Rab7 regulates late endocytic trafficking downstream of multivesicular body biogenesis and cargo sequestration. J Biol Chem 2009;284:12110–24.

[39] Wei D, Zhan W, Gao Y, Huang L, Gong R, Wang W, et al. RAB31 marks and controls an ESCRT-independent exosome pathway. Cell Res 2021;31:157–77.

[40] Sabbatinelli J, Matacchione G, Giuliani A, Ramini D, Rippo MR, Procopio AD, et al. Circulating biomarkers of inflammaging as potential predictors of COVID-19 severe outcomes. Mech Ageing Dev 2022;204:111667.

[41] Spiezia L, Boscolo A, Poletto F, Cerruti L, Tiberio I, Campello E, et al. COVID-19-Related Severe Hypercoagulability in Patients Admitted to Intensive Care Unit for Acute Respiratory Failure. Thromb Haemost 2020;120:998–1000.

[42] Ghebrehiwet B, Hosszu KH, Peerschke EI. C1q as an autocrine and paracrine regulator of cellular functions. Mol Immunol 2017;84:26–33.

[43] Castellano G, Woltman AM, Schena FP, Roos A, Daha MR, van Kooten C. Dendritic cells and complement: at the cross road of innate and adaptive immunity. Mol Immunol 2004;41:133–40.

[44] Tabatabai A, Rabin J, Menaker J, Madathil R, Galvagno S, Menne A, et al. Factor VIII and Functional Protein C Activity in Critically Ill Patients With Coronavirus Disease 2019: A Case Series. A A Pract 2020;14:e01236.

[45] Rauch A, Labreuche J, Lassalle F, Goutay J, Caplan M, Charbonnier L, et al. Coagulation biomarkers are independent predictors of increased oxygen requirements in COVID-19. J Thromb Haemost 2020;18:2942–53.

[46] Liu S, Zhu L, Xie G, Mok B-W-Y, Yang Z, Deng S, et al. Potential Antiviral Target for SARS-CoV-2: A Key Early Responsive Kinase during Viral Entry. CCS. Chemistry 2021:559–68.

[47] Kang SW, Wahl MI, Chu J, Kitaura J, Kawakami Y, Kato RM, et al. PKCbeta modulates antigen receptor signaling via regulation of Btk membrane localization. Embo j 2001;20:5692–702.

[48] Li Y-F, Lee K-G, Ou X, Lam K-P. Bruton's Tyrosine Kinase and Protein Kinase C μ Are Required for TLR7/9-Induced IKKα and IRF-1 Activation and Interferon-β Production in Conventional Dendritic Cells. PLoS One 2014;9:e105420.

[49] Gupta Y, Maciorowski D, Zak SE, Jones KA, Kathayat RS, Azizi SA, et al. Bisindolylmaleimide IX: A novel anti-SARS-CoV2 agent targeting viral main protease 3CLpro demonstrated by virtual screening pipeline and in-vitro validation assays. Methods 2021.

[50] Liu J-F, Zhou Y-N, Lu S-Y, Yang Y-H, Wu S-F, Liu D-P, et al. Proteomic and phosphoproteomic profiling of COVID-19-associated lung and liver injury: a report based on rhesus macaques. Signal Transduct Target Ther 2022;7:27.

[51] Strich JR, Tian X, Samour M, King CS, Shlobin O, Reger R, et al. Fostamatinib for the Treatment of Hospitalized Adults With Coronavirus Disease 2019: A Randomized Trial. Clin Infect Dis 2021;75:e491–8.

[52] Moon HG, Cao Y, Yang J, Lee JH, Choi HS, Jin Y. Lung epithelial cell-derived extracellular vesicles activate macrophage-mediated inflammatory responses via ROCK1 pathway. Cell Death Dis 2015;6:e2016.

[53] Abedi F, Rezaee R, Karimi G. Plausibility of therapeutic effects of Rho kinase inhibitors against Severe Acute Respiratory Syndrome Coronavirus 2 (COVID-19). Pharmacol Res 2020;156:104808.

[54] Xu XL, Shi LH, Ma XQ, Su H, Ma GF, Wu XH, et al. RhoA-Rho associated kinase signaling leads to renin-angiotensin system imbalance and angiotensin converting enzyme 2 has a protective role in acute pulmonary embolism. Thromb Res 2019; 176:85–94.

[55] Calò LA, Bertoldi G, Davis PA. Rho kinase inhibitors for SARS-CoV-2 induced acute respiratory distress syndrome: Support from Bartter's and Gitelman's syndrome patients. Pharmacol Res 2020;158:104903.

[56] Vicari RM, Chaitman B, Keefe D, Smith WB, Chrysant SG, Tonkon MJ, et al. Efficacy and safety of fasudil in patients with stable angina: a double-blind, placebo-controlled, phase 2 trial. J Am Coll Cardiol 2005;46:1803–11.

[57] Koch JC, Kuttler J, Maass F, Lengenfeld T, Zielke E, Bähr M, et al. Compassionate Use of the ROCK Inhibitor Fasudil in Three Patients With Amyotrophic Lateral Sclerosis. Front Neurol 2020;11.

[58] Rébillard R-M, Charabati M, Grasmuck C, Filali-Mouhim A, Tastet O, Brassard N, et al. Identification of SARS-CoV-2-specific immune alterations in acutely ill patients. J Clin Invest 2020.

[59] Zimmerman AW, Joosten B, Torensma R, Parnes JR, van Leeuwen FN, Figdor CG. Long-term engagement of CD6 and ALCAM is essential for T-cell proliferation induced by dendritic cells. Blood 2006;107:3212–20.

[60] Miao G, Zhao H, Li Y, Ji M, Chen Y, Shi Y, et al. ORF3a of the COVID-19 virus SARS-CoV-2 blocks HOPS complex-mediated assembly of the SNARE complex required for autolysosome formation. Dev Cell 2021;56(427–42):e5.

[61] Ghosh S, Dellibovi-Ragheb TA, Kerviel A, Pak E, Qiu Q, Fisher M, et al. beta-Coronaviruses Use Lysosomes for Egress Instead of the Biosynthetic Secretory Pathway. Cell 2020;183(1520–35):e14.

[62] Jae LT, Raaben M, Herbert AS, Kuehne AI, Wirchnianski AS, Soh TK, et al. Virus entry. Lassa virus entry requires a trigger-induced receptor switch. Science 2014; 344:1506–10.

[63] Cohen-Dvashi H, Israeli H, Shani O, Katz A, Diskin R. Role of LAMP1 Binding and pH Sensing by the Spike Complex of Lassa Virus. J Virol 2016;90:10329–38.